Cooperative Control of Online Impedance Spectroscopy Monitoring Method and Maximum Power Point Tracking Method for Photovoltaic Panels

Xin Wang*, Zhixue Zheng*, Michel Aillerie*, Alexandre De Bernardinis, Jean-Paul Sawicki
LABORATOIRE MATÉRIAUX OPTIQUES, PHOTONIQUE ET SYSTÈMES (LMOPS),
UNIVERSITÉ DE LORRAINE & CENTRALESUPÉLEC
Metz, France
* Corresponding authors: xin.wang@univ-lorraine.fr, zhixue.zheng@univ-lorraine.fr,
michel.aillerie@univ-lorraine.fr,
alexandre.de-bernardinis@univ-lorraine.fr,
jean-paul.sawicki@univ-lorraine.fr

Marie-Cécile Péra, Daniel Hissel
FCLAB, CENTRE NATIONAL DE LA RECHERCHE SCIENTIFIQUE (CNRS),
FRANCHE-COMTÉ ÉLECTRONIQUE MÉCANIQUE THERMIQUE ET OPTIQUE-
SCIENCES ET TECHNOLOGIES (FEMTO-ST) INSTITUTE, UNIVERSITÉ
BOURGOGNE FRANCHE-COMTÉ,
Belfort, France
marie-cecile.pera@univ-fcomte.fr,
daniel.hissel@univ-fcomte.fr

Acknowledgements

Authors gratefully thank the Chinese Scholarship Council (CSC) and French national research agency ANR in the framework of the EREMITE project (ANR-19-CE05-0008-01) for their financial support to the achievement of the work.

Keywords

«Photovoltaics», « Impedance measurement», «Control methods for electrical systems», «Solar Field»

Abstract

Health monitoring is essential for the photovoltaic (PV) panels to improve the system's efficiency and stability. Existing health monitoring methods are applied either offline or need additional equipment. Impedance spectroscopy (IS) methods can characterize online the internal processes of electrochemical systems with corresponding equivalent circuit model. However, it is rarely used for PV panels. This paper focuses on the online implementation of IS based on existing power converter for real-time health monitoring of PV panels. The injection region and type of perturbation signal for PV panels during IS measuring are analyzed. Based on PV panel's equivalent circuit model, a theoretical analysis of the influence of temperature and irradiance on internal parameters is made. Besides, a cooperative control method of online IS method and maximum power point tracking (MPPT) method is proposed. Even during the IS measuring, the quasi-maximum output power of PV panels can be maintained. The feasibility of the proposed method is verified by both simulation and experiment under different operating conditions.

Introduction

Due to the depletion of conventional energy sources and environmental impacts, the role of renewable sources for energy generation such as solar energy has become a prior choice nowadays [1]. As for other energetic sources and systems, health monitoring is essential for photovoltaic (PV) panels to detect the occurring faults and the degradation states, and to further improve the operational efficiency. The commonly used I-V curves of PV panels can provide fundamental electrical

information in the full operating voltage range. Based on these curves, the state of PV panels can be monitored and several typical faults such as partial shading, short circuit and natural degradation can be diagnosed [2]. However, during the voltage sweep which is necessary to obtain information about the health state of the panel, the output voltage varies from open circuit to short circuit. Hence, in micro-grid applications, the PV panels can no longer assure (quasi-) maximum output power during the tests [3]-[5]. Another diagnostic category is based on imaging techniques [6], such as infrared imaging, lock in thermography (LIT), and electroluminescence imaging. However, these techniques are either limited by their high cost or offline applications, which are not suitable for online small power-scale applications.

Impedance spectroscopy (IS) is a widely used diagnostic tool in electrochemical systems such as batteries and fuel cells in combination with their AC equivalent models [7]-[9]. The basic principle is to impose a small perturbation signal (current or voltage) over the operation point of tested system and measure the corresponding response signal (voltage or current). If a current perturbation is carried out, the mode is called "galvanostatic". Otherwise, if a voltage perturbation is applied, the mode is called "potentiostatic". The impedance information is then extracted and calculated to characterize the system. Compared with I-V curves and other detection tools, IS method has more advantages for health monitoring of PV panels as elements of a microgrid due to the following reasons:

- IS method is non-destructive. It doesn't require the disconnection of PV panels from the microgrid during the operation, while assures a quasi-maximum output power of PV panels. Thus, the full operational functionality of the system can be maintained.
- IS method is capable of capturing the dynamics of the PV panel operation and characterizing the internal processes. When combined with an AC equivalent circuit model, the internal representative parameters of PV panels can be extracted and used for online health monitoring.
- IS method can be easily implemented for embedded applications. There is no need of additional equipment (e.g., electrochemical workstation) when based on existing power converters.

In the literature, it has been verified that IS method can describe accurately the internal states of PV panels by comparing with results obtained from frequency response analyzers and commonly used I-V curves [10]-[17]. Based on a commercial electrochemical workstation Zahner IM6, internal parameters of a single PV cell were tested in [10]. Due to the limitation of measuring current (± 3 A) and voltage range (± 4 V), this method is only applicable for a single PV cell. A converter-based IS method was implemented and verified in [12] [13]. However, the IS measurements were either made at open-circuit voltages or were achieved by open-loop regulation of duty cycle of the converter. In summary, the online application of IS method for PV panels' health monitoring is still in its infancy.

This work carried out in the framework of the EREMITE project funded by the Chinese Scholarship Council (CSC) and French Research Agency (ANR), aims to implement the IS method based on an existing DC-DC converter. The integration of the IS function into the converter controller can achieve a smooth transition between two modes, i.e., traditional maximum power point tracking (MPPT) mode and IS mode. Consequently, an additional electrochemical workstation is no longer required. The efficiency and reliability of the PV panels can be optimized in an autonomous way. In section II, both static and dynamic models of PV panel are briefly introduced. The AC equivalent circuit model and the online implementation of IS method are emphasized in section III. The feasibility of the proposed methodology has been verified by simulation results based on MATLAB/Simulink. In Section IV, experiments are further performed to study the influences of operating temperature and irradiance levels on the IS measurements. Conclusions are drawn in the final section.

PV panel characteristics

PV panels are made of several types of semiconductors using different manufacturing processes. In general, a PV cell can be essentially considered as a *p-n* junction. Under the radiation of light, carries move between different layers, which leads to current flow into the external circuit. The output current is affected by temperature and irradiance that affect the number of charge carriers and the moving speeds.

In general, an equivalent static model is applied to characterize the performance of PV panels, as shown in Fig. 1 (a). R_s and R_{sh} represent the series and shunt resistances, respectively. V is the output voltage and I is output current. D is a Schottky diode, which allows to describe the influence of temperature and irradiance on the output current. However, the static model can only react with the resistance information (i.e., R_s and R_{sh}) of PV panel under static conditions. To characterize the dynamic performance of PV panels, an equivalent dynamic model is necessary. In this paper, a dynamic model in [19] was referenced, while the reverse-bias conduction mode isn't considered in our case. Hence, the equivalent dynamic model is further simplified as the circuit shown in Fig. 1 (b).

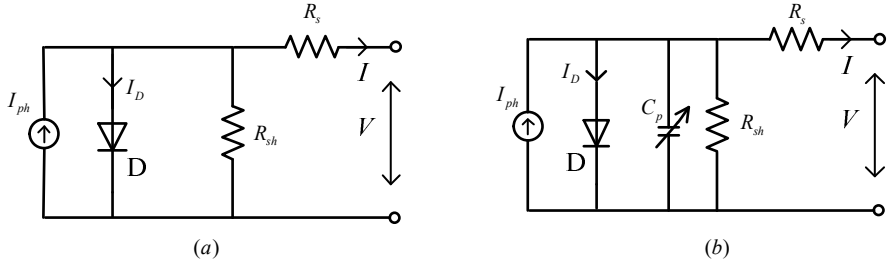

Fig. 1 (a) Equivalent static model; (b) Equivalent dynamic model

Compared with equivalent static model, a variable capacitor C_p is added in the dynamic model. And it can be expressed as follows:

$$C_p = \frac{q\tau I_D}{akT} \tag{1}$$

Where a is the ideality factor ($1 < a < 2$), q is the absolute value of electron's charge ($q = 1.6*10^{-19}$ C), k is the Boltzmann's constant ($k = 1.35*10^{-23}$ J/K), T is the Kelvin temperature of the panel and τ represents the lifetime of carriers inside of PV panel.

Based on the Kirchhoff's law, the output voltage and current can be expressed follows:

$$\begin{cases} I = I_{ph} - I_D - I_{C_p} - I_{R_{sh}} \\ V = V_D + I \cdot R_s \end{cases} \tag{2}$$

Where I_{ph}, I_{cp} and I_{Rsh} represent photovoltaic current, the current of C_p and R_{sh}, respectively. V_D is the direct voltage of the diode. And the equivalent resistance of the diode can be written as:

$$R_D = V_D / I_D \tag{3}$$

To achieve a high energy generation efficiency, an MPPT method for PV systems is necessary. There are numerous MPPT methods proposed in the existing literature. In this paper, a traditional perturbation and observation (P&O) method is considered [18]. Since this work focuses majorly on the online IS method, more details on the MPPT methods will not be given herein.

Online Impedance Spectroscopy Method

For small and medium power distributed systems, PV modules are commonly equipped with an optimizer with MPPT function and a power converter. This section introduces an online implementation method to obtain the IS measurements based on its connected converter.

AC equivalent circuit of PV panels

An AC equivalent circuit is required for interpreting the IS measurements. Based on the equivalent dynamic model a corresponding AC equivalent circuit of PV panel is drawn in Fig. 2 (a). The model describes a Nyquist plot with a single time constant of R_p in parallel with a capacitor C_p, which is

shifted from the origin by a series resistance R_s. R_p represents the associated recombination resistance of R_{sh} and R_D in Fig. 1 (b).

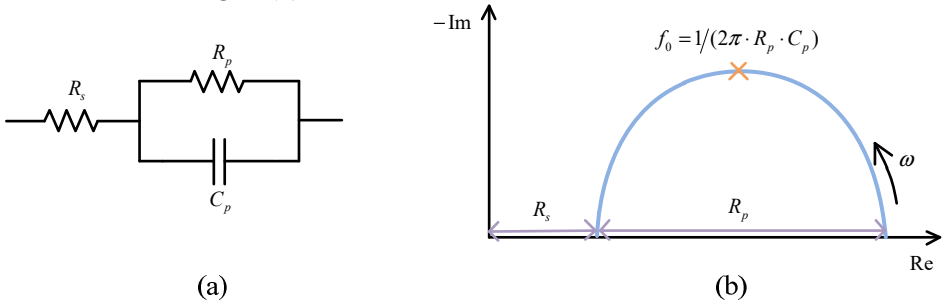

Fig. 2 (a) AC equivalent circuit model connected with a boost converter; (b) An ideal Nyquist curve with several representative parameters

By imposing a small voltage/current perturbation over the operating point of the tested system and measuring the corresponding current/voltage response, the Nyquist curve of PV panel can be obtained, which contains the impedance information over a large frequency range. As shown in Fig. 2 (b), the parameters of PV panels can be further extracted based on the Nyquist curve, where f_0 is the frequency of the top point of the curve and ω represents the angular frequency. The internal states of PV panel can thus be monitored by real-time IS measurements.

Online control method

The system controller setup is shown in Fig. 3 (*a*), including MPPT and IS method. In this setup, an AC current perturbation signal (i.e., the galvanostatic mode) is injected to achieve the IS measuring. The detail of the control loop for tracking the AC perturbation signal is shown in Fig. 3 (*b*), where $i_{\_ref\_ac}$ represents the reference the perturbation signal, I_0 is the DC component of output current, $i_{\_ref}$ is the sum of $i_{\_ref\_ac}$ and I_0, K_{PWM} is the gain of the converter's regulation, the equivalent impedance in s region is written as $sL+R_L$, and G(s) is the transfer function of controller used in Fig. 3 (*a*). The transfer function of the control block in Fig. 3 (*b*) can be expressed as follows:

$$\varphi(s) = \frac{I_{PV}(s)}{I_{\_ref}(s)} = \frac{G(s) \cdot K_{PWM} / (sL + R_L)}{1 + G(s) \cdot K_{PWM} / (sL + R_L)} \tag{4}$$

In our system, a PI controller ($G(s) = K_p + K_i/s$) is used, whose appropriate parameters can be obtained based on the Bode diagram of the transfer function. In this control block, considering the frequency of the AC perturbation, the values of K_p and K_i are set to 400 and 100 respectively. Under this set of parameters, the controller frequency bandwidth can reach 10 kHz, as shown in Fig. 3 (*c*).

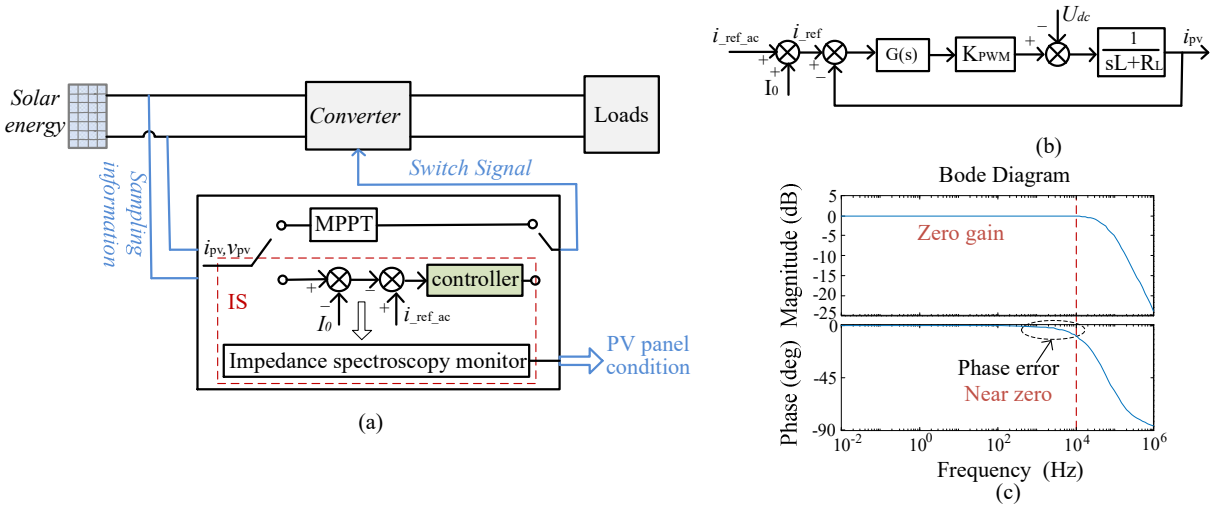

Fig. 3 (a) PV system with integrated IS method; (b) Control loop of IS online measurement

Simulation results

Based on the AC equivalent circuit in Fig. 2 (a) and the control method in Fig. 3, the cooperative control of online IS monitoring method and MPPT method is verified in MATLAB/Simulink. And the simulated results are shown in Fig. 4. The value of the DC bus voltage is set to 60 V and the switching frequency is equal to 10 *k*Hz.

In Fig. 4 (a), based on the changing rate of I_{pv}, I-V curve is divided into one non-linear region (II) and two quasi-linear regions (I and III). According to the validity condition of IS measurements in [20], the injecting region must be a linear or quasi-linear region, in order to fulfill the linearity condition. Hence, the two quasi-linear regions (I and III) can be chosen initially for AC signal injection.

In region I, taking P_{qi} as an injection point, it can be observed that a significant voltage perturbation signal in the potentiostatic mode is required in order to produce a measurable current response signal. In the galvanostatic mode, a sufficient AC current perturbation signal is difficult to reach, since the current variation range is relatively narrow in this region.

In region III, taking P_{qv} as an injecting point, it can be observed that due to the relatively large voltage variation range, it would be more flexible to implement either the potentiostatic mode or the galvanostatic mode. Concrete analysis of the injection mode will be further made based on measured I-V curves in section IV.

In Fig. 4 (b), PV panel operates in MPPT mode at the beginning; then the scanning is started to achieve IS measuring. Once the scanning is completed, the PV panel continues to operate in MPPT mode. As can be seen in the responses, during the whole scanning process, PV panels are always connected with the microgrid bus and maintain an output power. Compared with MPPT process, the output power decreases little during IS measuring process (less than 5% of maximum P_{out}). Hence, IS method can assure a quasi-maximum PV output power during health monitoring.

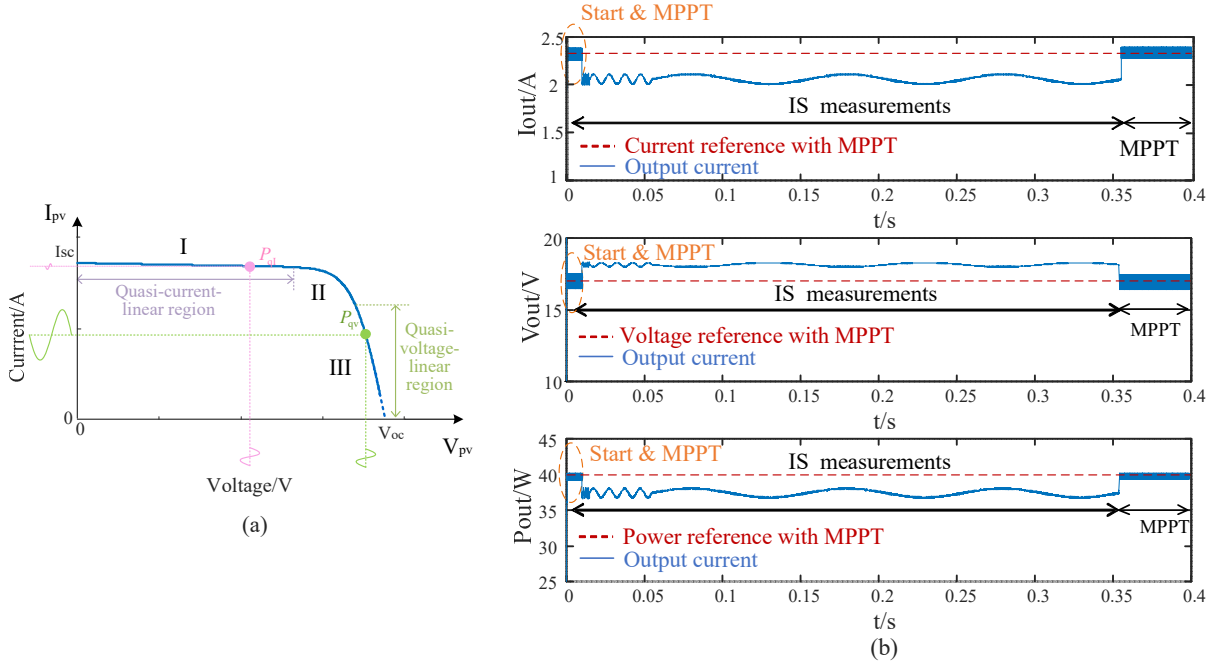

Fig. 4 (a) Region defined on I-V curve; (b) Simulation waveforms of the PV panel output current, voltage and power operating under the proposed control method

Experimental validation

Based on the proposed control method, experiments are performed to test the influence of temperature and irradiance to a PV panel in the laboratory. The experimental platform is shown in Fig. 5. A homemade magnetically coupled boost (MCB) converter was utilized herein, due to its high step-up

ratio (up to 10) and high efficiency (> 92%) [21]. The output current is acquired by a high-accuracy and wide bandwidth current transducer (IT 65-S ULTRASTAB. The operating temperature is measured by a thermal camera (FILR E8) as shown in Fig. 5(b) and an average surface temperature is taken for information. The irradiance level is measured by a solar power meter PYR 1307.

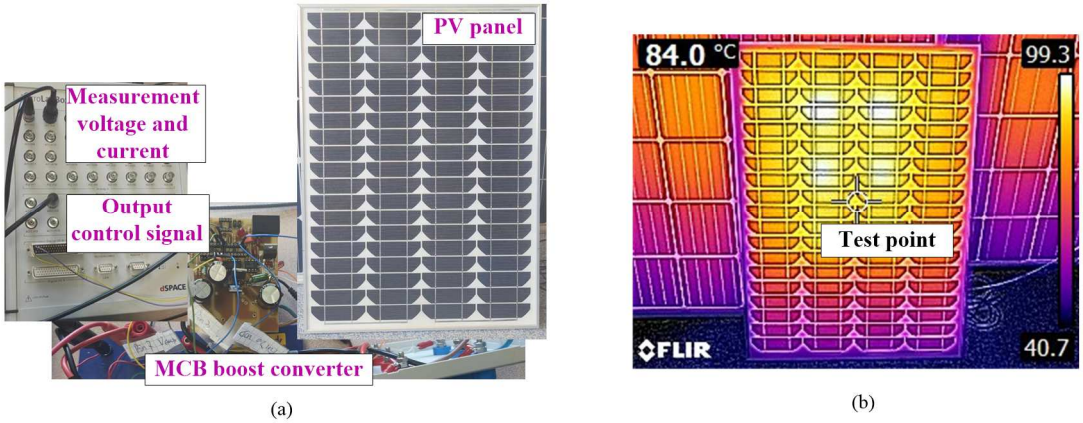

(a) (b)

Fig. 5 (a) Experimental platform; (b) Operating temperature based on FLIS E8

A set of I-V curves under different operating temperatures with the same irradiance are shown in Fig. 6 (a). And a group of I-V curves under different irradiances with the same operating temperature are shown in Fig. 6 (b). If the potentiostatic mode is chosen, a common voltage injection point should be found for I-V curves at different operating temperatures. As can be observed in Fig. 6 (a), the PV panel output voltage is highly sensitive to changes of operating temperature especially in the quasi-voltage-linear region (region III). When the operating temperature changes significantly, it will be difficult to find a common injection point to pass through the region III of all the I-V curves. Taking P_{qv} (V_{pv} = 17 V) as an injection point, it can be observed that P_{qv} is in the nonlinear region II of I-V curve at 55 ºC (at P_{MPP}), while it is out of the voltage range of the I-V curve at 84 ºC. Meanwhile, for the galvanotactic mode, there is no such limitation. A common current injection point can be easily found while assures its location in region III, e.g., P_{1T}, P_{2T}, P_{3T} in Fig. 6 (a).

Under the influence of irradiance, the short circuit current (I_{sc}) is highly sensitive to the changes of irradiance, while the PV panel output voltage in region III keeps basically coincident among different curves, as shown in Fig. 6 (b). In this case, it would be easier to find a common current injection point. Therefore, the galvanostatic mode may be preferred. But if a common voltage injection point can be found, the potentiostatic mode can also be chosen, e.g., P_{1G}, P_{2G}, P_{3G} in Fig. 6 (b).

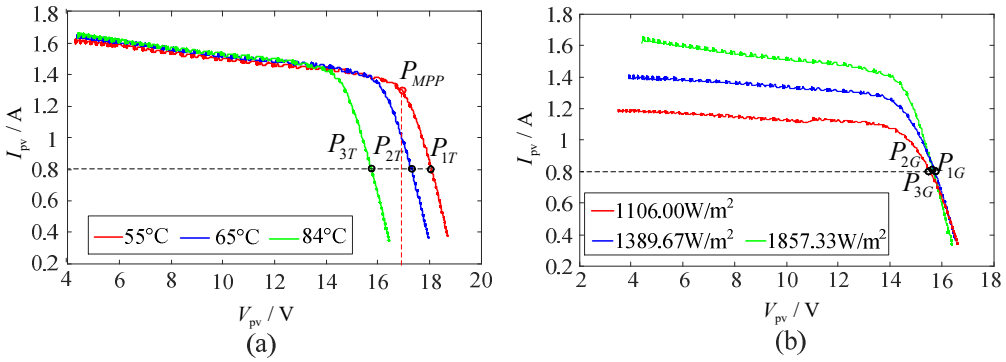

(a) (b)

Fig. 6 Experimental injecting points: (a) inject current-perturbation signal; (b) inject voltage-perturbation signal

In accordance with proposed control method, Nyquist curves and bode diagrams of different operating temperatures and irradiances are obtained and shown in Fig. 7 and Fig. 9, respectively. A free EIS analyzer is utilized to extract the parameters to AC equivalent circuit, shown as R_s, R_p and C_p in Table I and Table II. And the changes of all parameters under different operating condition are shown in Fig.

8 and Fig. 10. In addition, the total resistance information under static condition is given for comparison, by calculating the slope at the injection point of each I-V curve, shown as R_{IV} in Table I and Table II. In principle, there exists an equivalence between R_{IV} and the total equivalent resistance (R_s+R_p) of IS measurements when the injection signal frequency is very low (thus can be regarded as quasi-static condition).

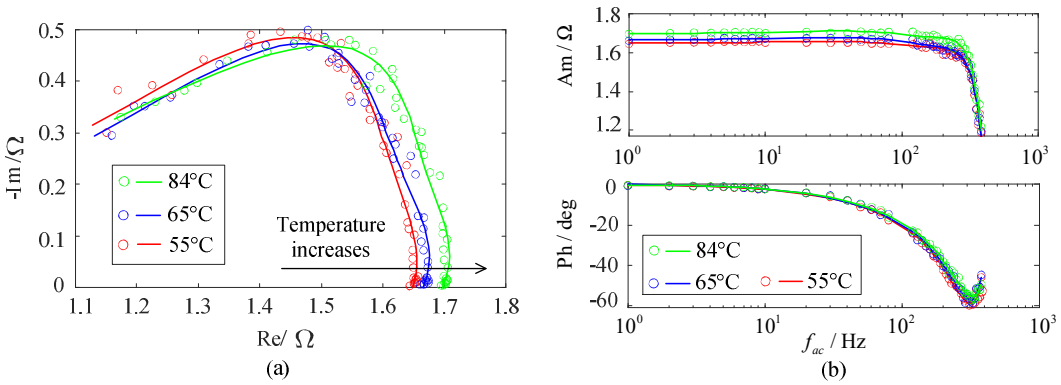

Fig. 7 Experimental results of different operating temperatures: (a) Nyquist curves; (b) Bode diagrams

As the operating temperature or irradiance change, a good consistency between the total equivalent resistance (R_s+R_p) and R_{IV} can be observed, as shown in Fig. 8 (a) and Fig. 10 (a). The error between the two resistances is less than 7%, which shows a good coherence between I-V curves and IS measurements at low frequencies. In parallel with the total equivalent resistance, IS measurement can equally provide equivalent capacitance information and separated resistance information of R_s and R_p, which is more powerful than I-V curves for health monitoring. As shown in Fig. 8 (b), R_p decreases with the increase of operating temperature, while R_s increases. When the irradiance increases, both R_p and R_s decrease as shown in Fig. 10 (b).

Table I: Internal parameters of PV panel at different operating temperatures

Temperature T (°C)	Equivalent Resistance in series R_s (Ω)	Equivalent Resistance in parallel R_p (Ω)	Total Equivalent Resistance R_s+R_p (Ω)	Equivalent Capacitance in parallel C_p (uF)	Total Equivalent Resistance on I-V curves R_{IV} (Ω)
55	0.76	0.92	1.68	397.98	1.69
65	0.82	0.88	1.70	438.43	1.71
84	0.87	0.86	1.73	398.15	1.73

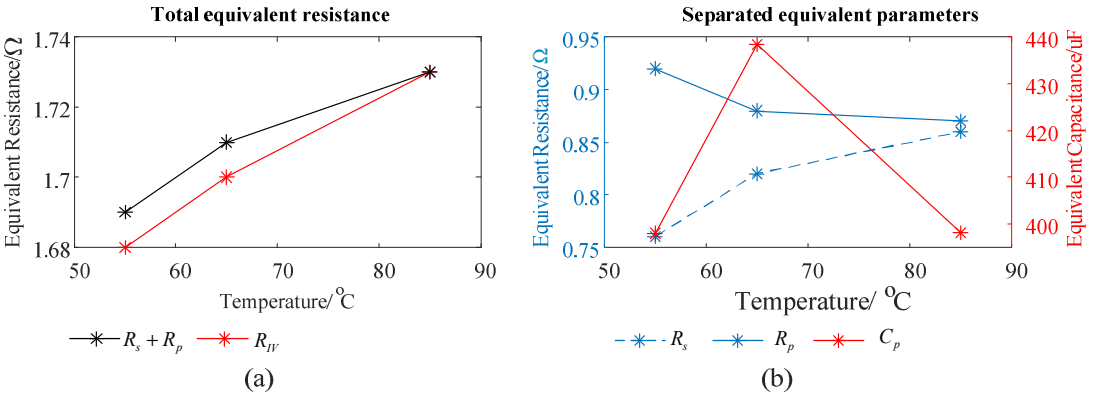

Fig. 8 Parameters' changing trend under different irradiances

When the operating temperature increases, the short circuit current (I_{sc}) is lightly affected while the output voltages of different injecting points (V_{P1T}, V_{P2T}, V_{P3T}) decrease significantly, as shown in Fig. 6 (a). Based on equation (2), the value of I_D is nearly constant while the value of V_D decreases as the operating temperature increases. Hence, the value of R_D will decrease. Since R_p is recombined by R_D and R_{sh}, its value will decrease the same as shown in Fig. 8 (b).

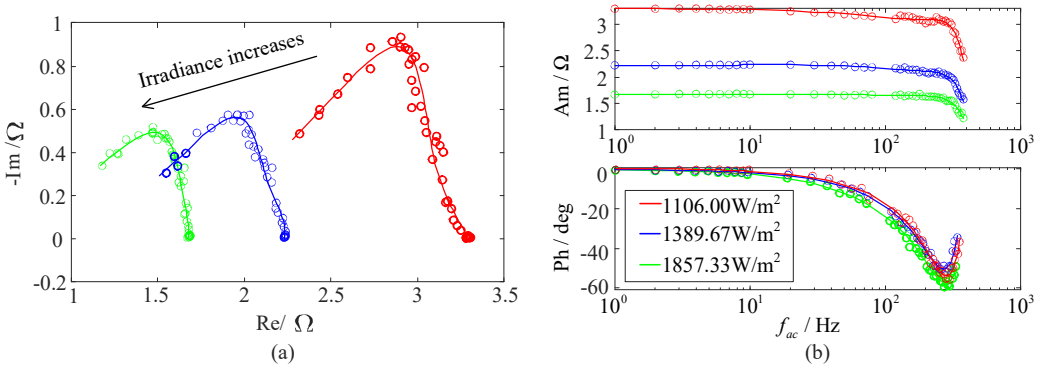

Fig. 9 Experimental results of different irradiances: (a) Nyquist curves; (b) Bode diagrams

When the irradiance increases, I_{sc} increases obviously as shown in Fig. 6 (b). In this condition, the output voltage of different injecting points (V_{P1G}, V_{P2G}, V_{P3G}) can be seen as a similar value. On the basis of equation (2), the value of I_D increases while the value of V_D is constant as the irradiance increases. R_p is composed of R_D and R_{sh} in parallel. The decrease of R_D will cause the value of R_p decreases, as shown in Fig. 10 (b).

Table II: Internal parameters of PV panel under different irradiances

Irradiance G (W/m^2)	Equivalent Resistance in series R_s (Ω)	Equivalent Resistance in parallel R_p (Ω)	Total Equivalent Resistance R_s+R_p (Ω)	Equivalent Capacitance in parallel C_p (uF)	Total Equivalent Resistance on I-V curves R_{IV} (Ω)
1857.33	0.75	0.96	1.71	373.91	1.83
1389.67	1.27	0.98	2.25	464.78	2.23
1106.00	1.73	1.56	3.29	253.26	3.21

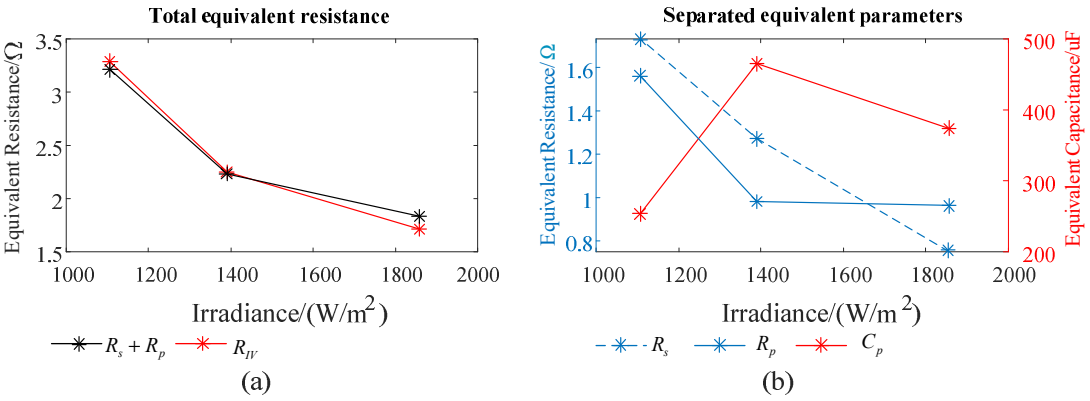

Fig. 10 Parameters' changing trend under different irradiances

According to the experimental results, it can be concluded that: when the irradiance changes, the values of R_p and R_s have the same changing trend; when the operating temperature changes, the values of R_p and R_s have the opposite changing trend. Based on the information of internal parameters obtained from IS measurement, the different operating conditions (i.e., different operating temperatures and irradiances herein) of PV panel can be identified.

Conclusion

In this paper, the online health monitoring of PV panels is emphasized. A collaborative control method between the MPPT and the IS measuring modes is proposed. Real-time measurements of IS based on DC-DC converter can be realized without the requirement of additional special equipment. Based on the AC equivalent circuit model, the internal parameters of PV panel under different operating temperatures and irradiances can thus be extracted and further utilized for online health monitoring. In the next step, IS measurements under different fault scenarios will be further focused on. If used for fault detection, different frequency segments relative to different types of faults can be divided to reduce unnecessary frequency measurements. Meanwhile, it can be noticed that the DC-DC converter design (e.g., the semiconductor material, its topology, and parameters) will affect the bandwidth of system control loop. And its influence to IS measurement will be additionally researched in the next step.

References

[1] V. Narayanan, S. Kewat, and B. Singh, "Solar PV-BES Based Microgrid System with Multifunctional VSC," IEEE Transactions on Industry Applications, vol. 56, no. 3, pp. 2957–2967, 2020

[2] Z. Zhang, M. Ma, H. Wang, H. Wang, W. Ma, and X. Zhang, "A fault diagnosis method for photovoltaic module current mismatch based on numerical analysis and statistics," Solar Energy, vol. 225, no. July, pp. 221–236, 2021

[3] A. Eskandari, J. Milimonfared, and M. Aghaei, "Line-line fault detection and classification for photovoltaic systems using ensemble learning model based on I-V characteristics," Solar Energy, vol. 211, no. July, pp. 354–365, 2020

[4] F. You and J. Benedikt, "An optimized-load-impedance calculation and mining method based on I-V Curves: Using broadband class-E power amplifier as example," IEEE Transactions on Industrial Electronics, vol. 66, no. 7, pp. 5254–5263, 2019

[5] B. Zbib and H. Al Sheikh, "Fault Detection and Diagnosis of Photovoltaic Systems through I-V Curve Analysis," 2nd International Conference on Electrical, Communication and Computer Engineering, ICECCE 2020, no. June, pp. 12–13, 2020

[6] K. Abdulmawjood, S. S. Refaat, and W. G. Morsi, "Detection and prediction of faults in photovoltaic arrays: A review," Proceedings - 2018 IEEE 12th International Conference on Compatibility, Power Electronics and Power Engineering, CPE-POWERENG 2018, pp. 1–8, 2018

[7] M. Crescentini et al., "Online EIS and Diagnostics on Lithium-Ion Batteries by Means of Low-Power Integrated Sensing and Parametric Modeling," IEEE Transactions on Instrumentation and Measurement, vol. 70, 2021

[8] H. Wang, A. Gaillard, and D. Hissel, "A review of DC/DC converter-based electrochemical impedance spectroscopy for fuel cell electric vehicles," Renewable Energy, vol. 141, pp. 124–138, 2019

[9] A Narjiss, D. Depernet, D. Candusso, F. Gustin, and D. Hissel, "On-line diagnosis of a PEM fuel cell through the PWM converter," Proceedings of FDFC 2008, pp. 734–739, 2008.

[10] D. Depernet, J. Vernier, P.A. Gril. Caractérisation de panneaux photovoltaïques par mesure d'impédance. Symposium de Génie Electrique, Université de Lorraine [UL], Nancy, France, 2018.

[11] D. Chenvidhya, K. Kirtikara, and C. Jivacate, "A new characterization method for solar cell dynamic impedance," Solar Energy Materials and Solar Cells, vol. 80, no. 4, pp. 459–464, 2003

[12] O. I. Olayiwola and P. S. Barendse, "Power Electronic Implementation of Electrochemical Impedance Spectroscopy on Photovoltaic Modules," ECCE 2020 - IEEE Energy Conversion Congress and Exposition, pp. 3654–3661, 2020

[13] M. A. Varnosfaderani and D. Strickland, "Online Electrochemical Impedance Spectroscopy (EIS) estimation of a solar panel," Vacuum, vol. 139, pp. 185–195, 2017

[14] S. Osawa, T. Nakano, S. Matsumoto, N. Katayama, Y. Saka, and H. Sato, “Fault diagnosis of photovoltaic modules using AC impedance spectroscopy,” 2016 IEEE International Conference on Renewable Energy Research and Applications, ICRERA 2016, vol. 5, pp. 210–215, 2017

[15] M. Lohrasbi, P. Pattanapanishsawat, M. Isenberg, and S. S. C. Chuang, “Degradation study of dye-sensitized solar cells by electrochemical impedance and FTIR spectroscopy,” 2013 IEEE Energytech, Energytech 2013, pp. 13–16, 2013

[16] M. I. Oprea, S. V. Spataru1, D. Sera, P. B. Poulsen, S. Thorsteinsson, R. Basu, A. R. Andersen, K. H.B. Frederiksen., “Detection of potential induced degradation in c-Si PV panels using electrical impedance spectroscopy,” Conference Record of the IEEE Photovoltaic Specialists Conference, vol. 2016-November, no. 2, pp. 1575–1579, 2016

[17] O. I. Olayiwola and P. S. Barendse, “Characterization of Silicon-Based Photovoltaic Cells Using Broadband Impedance Spectroscopy,” IEEE Transactions on Industry Applications, vol. 54, no. 6, pp. 6309–6319, 2018

[18] T. Esram and P. L. Chapman, “Comparison of photovoltaic array maximum power point tracking techniques,” IEEE Transactions on Energy Conversion, vol. 22, no. 2, pp. 439–449, 2007.

[19] K. A. Kim, C. Xu, L. Jin, and P. T. Krein, “A dynamic photovoltaic model incorporating capacitive and reverse-bias characteristics,” IEEE Journal of Photovoltaics, vol. 3, no. 4, pp. 1334–1341, 2013.

[20] X.-Z. Yuan, S. Chaojie, W. Haijiang, Z. Jiujun, Electrochemical Impedance Spectroscopy in PEM Fuel Cells: Fundamentals and Applications (Springer, London, 2010), pp. 95–136

[21] P. Petit, M. Aillerie, J. P. Sawicki, and J. P. Charles, “High efficiency DC-DC converters including a performed recovering leakage energy switch,” Energy Procedia, vol. 36, pp. 642–649, 2013.